Acta Cryst. (1977). A33, 740–749

A New Theoretical and Practical Approach to the Multislice Method

BY KAZUO ISHIZUKA AND NATSU UYEDA

Institute for Chemical Research, Kyoto University, Uji, Kyoto-Fu 611, *Japan*

(*Received* 1 *October* 1976; *accepted* 8 *April* 1977)

The multislice formulation of Cowley and Moodie for high-energy electron scattering is rederived from the Schrödinger equation, and the validity of the finite slice approach in practical computation is theoretically proved by the stationary-phase approximation. A set of computer programs for the multislice method is developed, where the convolution integral is carried out through the fast Fourier transform. The following conditions are required to obtain a sufficiently accurate result in multislice calculations: (1) the maximum slice thickness should be about kd^2, where k is the wavenumber of the incident electrons and d is the distance over which the potential does not change appreciably; (2) there must be a sufficient number of beams in the multislice iteration to prevent the aliasing effect of convolution. The multiple scattering masks the real specimen structure when the specimen thickness exceeds a certain value. This effect of multiple scattering is recognized from the probability distribution of the scattered electrons in addition to the scattering amplitudes obtained through the procedure developed in the present work.

I. Introduction

Cowley & Moodie (1957) formulated the multislice method for the n-beam dynamical electron scattering in an analogy to classical optics. It was shown by Goodman & Moodie (1974) that, in the limiting case of zero slice thickness, this formulation is identical to the Schrödinger equation which rules the behaviour of electrons. Extensive applications of this method to two-dimensional problems, facilitated by the electronic digital computer, have been made by the Australian school in the series *n-Beam Lattice Images* (Allpress, Hewat, Moodie & Sanders, 1972; Lynch & O'Keefe, 1972; Anstis, Lynch, Moodie & O'Keefe, 1973; O'Keefe, 1973; Lynch, Moodie & O'Keefe, 1975; O'Keefe & Sanders, 1975). Goodman & Moodie (1974) summarized the computing technique where convolution integrals are directly calculated.

In this paper, the multislice formula is derived directly from the integral form of the Schrödinger equation. This integral equation is first replaced by a function similar to the infinite Born series (Schiff, 1956; Fujiwara, 1959), and solved by applying the method of stationary phase (Eckart, 1948) to each term. A new practical computing technique is developed where the convolution integrals are carried out through Fourier transforms on the basis of the Fourier theorem of convolution. The effects of the number of beams and of the slice thickness on the multislice calculation are discussed in terms of this newly developed computing technique.

II. Theoretical

2.1 *Derivation of the multislice formula on the basis of the Schrödinger equation*

In the Cartesian coordinate system, the Schrödinger equation is written as

$$(\nabla^2+k^2)\psi(\mathbf{r})=\frac{2m}{\hbar^2}V(\mathbf{r})\,.\,\psi(\mathbf{r}), \tag{1}$$

where $k=|\mathbf{k}|$, $\mathbf{k}$ is the wavevector of the incident electrons, $V(\mathbf{r})$ is the potential energy, and $\mathbf{r}=(x,y,z)$. The solution of this equation is usually given in the following integral form:

$$\psi(\mathbf{r})=\exp(i\mathbf{kr})-\frac{2m}{4\pi\hbar^2}\int\frac{\exp(ik|\mathbf{r}-\mathbf{r}'|)}{|\mathbf{r}-\mathbf{r}'|}V(\mathbf{r}')\,.\,\psi(\mathbf{r}')\mathrm{d}\mathbf{r}'. \tag{2}$$

If the wave function is expressed by the product of the incident plane wave and a factor $\varphi(\mathbf{r})$ which describes a modulation on the incident wave as

$$\psi(\mathbf{r})=\exp(i\mathbf{kr})\varphi(\mathbf{r}), \tag{3}$$

then (2) is rewritten in terms of φ as:

$$\varphi(\mathbf{r})=1-\frac{2m}{4\pi\hbar^2}\int\frac{\exp i\{k|\mathbf{r}-\mathbf{r}'|-\mathbf{k}(\mathbf{r}-\mathbf{r}')\}}{|\mathbf{r}-\mathbf{r}'|}\times V(\mathbf{r}')\,.\,\varphi(\mathbf{r}')\mathrm{d}\mathbf{r}'. \tag{4}$$

When the high-energy electron scattering satisfies the following condition:

$$\alpha^2\ll 1\ (\alpha;\text{ the scattering angle}),$$

the small-angle approximation holds and

$$|\mathbf{r}-\mathbf{r}'|\simeq z-z'.$$

Thus

$$k|\mathbf{r}-\mathbf{r}'|-\mathbf{k}(\mathbf{r}-\mathbf{r}')\simeq k\frac{|\mathbf{b}-\mathbf{b}'|^2}{2(z-z')}.$$

Here the two vectors $\mathbf{b}=(x,y)$ and $\mathbf{b}'=(x',y')$ are perpendicular to the incident electrons, *i.e.* z-axis (see Fig. 1). Equation (4) is approximated for the forward scattering as

$$\varphi(\mathbf{b},z)=1-\int\int_{z'=-\infty}^{z'=z}\frac{i}{\hbar v}V(\mathbf{b}',z')\,.\,\varphi(\mathbf{b}',z')\times\left[\frac{1}{z-z'}\,\frac{1}{\lambda i}\exp\left\{ik\frac{|\mathbf{b}-\mathbf{b}'|^2}{2(z-z')}\right\}\right]\mathrm{d}z'\mathrm{d}\mathbf{b}'. \tag{5}$$

Here the relationship

$$\frac{2m}{4\pi\hbar^2}=\frac{i}{\hbar v}\frac{1}{\lambda i}$$

is used, and v is the velocity of the incident electrons. The term in the square brackets describes the wave propagation between two points $\mathbf{r}=(\mathbf{b},z)$ and $\mathbf{r}'=(\mathbf{b}',z')$ and is defined as the propagation function (Cowley & Moodie, 1957), which will be denoted by $p(\mathbf{b},z)$ hereafter:

$$p(\mathbf{b},z)=\frac{1}{z}\frac{1}{\lambda i}\exp\left\{ik\frac{|\mathbf{b}|^2}{2z}\right\}. \tag{6}$$

$p(\mathbf{b},z)$ has the form of the Huygens wavelet within the paraboloidal approximation, and has the following property, like a diffraction integral over the plane Σ positioned at z'' between z and z':

$$p(\mathbf{b}-\mathbf{b}',z-z')=\int_{\Sigma}p(\mathbf{b}-\mathbf{b}'',z-z'')p(\mathbf{b}''-\mathbf{b}',z''-z')\mathrm{d}\mathbf{b}''. \tag{7a}$$

Here $p(\mathbf{b},z)$ is normalized as

$$\int p(\mathbf{b},z)\mathrm{d}\mathbf{b}=1. \tag{7b}$$

With these relations (7a) and (7b) of the propagation function, (5) will be modified as follows:

$$\begin{aligned}\varphi(\mathbf{b},z)=&1+\left(-\frac{i}{\hbar v}\right)\int_{V_{\mathrm{I}}}\int_{z''=-\infty}^{z''=z_0}V(\mathbf{b}'',z'')\varphi(\mathbf{b}'',z'')\\&\times p(\mathbf{b}-\mathbf{b}'',z-z'')\mathrm{d}z''\mathrm{d}\mathbf{b}''\\&+\left(-\frac{i}{\hbar v}\right)\int_{V_{\mathrm{II}}}\int_{z'=z_0}^{z'=z}V(\mathbf{b}',z')\varphi(\mathbf{b}',z')\\&\times p(\mathbf{b}-\mathbf{b}',z-z')\mathrm{d}z'\mathrm{d}\mathbf{b}'\\=&\int\left\{1+\left(-\frac{i}{\hbar v}\right)\int_{V_{\mathrm{I}}}\int_{z''=-\infty}^{z''=z_0}V(\mathbf{b}'',z'')\right.\\&\left.\times\varphi(\mathbf{b}'',z'')p(\mathbf{b}_0-\mathbf{b}'',z_0-z'')\mathrm{d}z''\mathrm{d}\mathbf{b}''\right\}\\&\times p(\mathbf{b}-\mathbf{b}_0,z-z_0)\mathrm{d}\mathbf{b}_0\\&+\left(-\frac{i}{\hbar v}\right)\int_{V_{\mathrm{II}}}\int_{z'=z_0}^{z'=z}V(\mathbf{b}',z')\varphi(\mathbf{b}',z')\\&\times p(\mathbf{b}-\mathbf{b}',z-z')\mathrm{d}z'\mathrm{d}\mathbf{b}'\\=&\int\varphi(\mathbf{b}_0,z_0)p(\mathbf{b}-\mathbf{b}_0,z-z_0)\mathrm{d}\mathbf{b}_0\\&+\left(-\frac{i}{\hbar v}\right)\int_{V_{\mathrm{II}}}\int_{z'=z_0}^{z'=z}V(\mathbf{b}',z')\varphi(\mathbf{b}',z')\\&\times p(\mathbf{b}-\mathbf{b}',z-z')\mathrm{d}z'\mathrm{d}\mathbf{b}'.\end{aligned} \tag{8}$$

This integral equation of Volterra's type (Margenau & Murphy, 1943) is solved by expanding $\varphi(\mathbf{b},z)$ in an infinite series:

$$\varphi(\mathbf{b},z)=\sum_{n=0}^{\infty}\left(-\frac{i}{\hbar v}\right)^n f_n(\mathbf{b},z). \tag{9}$$

The following set of equations is obtained by equating the coefficients of $(-i/\hbar v)^n$ on the two sides of (8) after substituting (9) into (8):

$$f_0(\mathbf{b},z)=\int\varphi(\mathbf{b}_0,z_0)p(\mathbf{b}-\mathbf{b}_0,z-z_0)\mathrm{d}\mathbf{b}_0, \tag{10a}$$

$$\begin{aligned}f_n(\mathbf{b},z)=&\int\int_{z'=z_0}^{z'=z}V(\mathbf{b}',z')f_{n-1}(\mathbf{b}',z')\\&\times p(\mathbf{b}-\mathbf{b}',z-z')\mathrm{d}z'\mathrm{d}\mathbf{b}',\quad n=1,2,3,\ldots.\end{aligned} \tag{10b}$$

For the potential varying slowly over the distance of order $\{(z-z_0)/k\}^{1/2}$, f_1 becomes

$$\begin{aligned}f_1(\mathbf{b},z)=&\int\int\int_{z'=z_0}^{z'=z}V(\mathbf{b}',z')\varphi(\mathbf{b}_0,z_0)p(\mathbf{b}'-\mathbf{b}_0,z'-z_0)\\&\times p(\mathbf{b}-\mathbf{b}',z-z')\mathrm{d}z'\mathrm{d}\mathbf{b}'\mathrm{d}\mathbf{b}_0\\=&\int\int_{z'=z_0}^{z'=z}V\left(\frac{(z'-z_0)\mathbf{b}+(z-z')\mathbf{b}_0}{z-z_0}\right)\\&\times\varphi(\mathbf{b}_0,z_0)p(\mathbf{b}-\mathbf{b}_0,z-z_0)\mathrm{d}z'\mathrm{d}\mathbf{b}_0\end{aligned} \tag{11}$$

after the integration over $\mathbf{b}'$ by the method of stationary phase (Appendix). If the potential varies slowly in the region of $(z-z_0)\cdot\alpha$, f_1 finally becomes

$$\begin{aligned}f_1(\mathbf{b},z)=&\int\left\{\int_{z'=z_0}^{z'=z}V(\mathbf{b}_0,z')\mathrm{d}z'\right\}\\&\times\varphi(\mathbf{b}_0,z_0)p(\mathbf{b}-\mathbf{b}_0,z-z_0)\mathrm{d}\mathbf{b}_0.\end{aligned} \tag{12a}$$

With the successive application of the stationary-phase method (Appendix), f_n reduces to

$$\begin{aligned}f_n(\mathbf{b},z)=&\int\frac{1}{n!}\left\{\int_{z'=z_0}^{z'=z}V(\mathbf{b}_0,z')\mathrm{d}z'\right\}^n\\&\times\varphi(\mathbf{b}_0,z_0)p(\mathbf{b}-\mathbf{b}_0,z-z_0)\mathrm{d}\mathbf{b}_0.\end{aligned} \tag{12b}$$

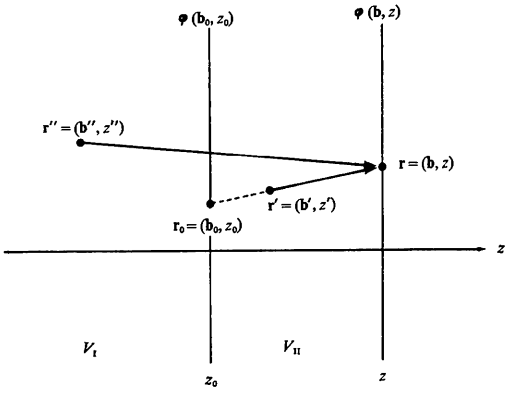

Fig. 1. A derivation of the multislice formula from an integral form of the Schrödinger equation. The region of integration in the forward-scattering approximation will be divided into two parts: V_{I} in front of and V_{II} inside the slice.

When (10*a*), (12*a*) and (12*b*) are substituted into (9), φ becomes

$$\varphi(\mathbf{b},z)=\int\exp\left\{-\frac{i}{\hbar v}\int_{z'=z_0}^{z'=z}V(\mathbf{b}_0,z')\mathrm{d}z'\right\}\times\varphi(\mathbf{b}_0,z_0)p(\mathbf{b}-\mathbf{b}_0,z-z_0)\mathrm{d}\mathbf{b}_0 \quad (13a)$$

after the summation over n. Equation (13*a*) is simply formulated by the convolution integral (denoted by $*$) as

$$\varphi_{n+1}(\mathbf{b})=[\varphi_n(\mathbf{b})\,.\,q_n(\mathbf{b})]*p(\mathbf{b},z_{n+1}-z_n)\,. \quad (13b)$$

Here the following simplified notations are used:

$$\varphi_n(\mathbf{b})=\varphi(\mathbf{b},z_n), \quad (14a)$$

$$q_n(\mathbf{b})=\exp\left\{-\frac{i}{\hbar v}\int_{z'=z_n}^{z'=z_{n+1}}V(\mathbf{b},z')\mathrm{d}z'\right\}. \quad (14b)$$

The sequence of the wave propagation and the phase shift by q in (13*b*) is in the reverse order to that in the Cowley–Moodie equation (Goodman & Moodie, 1974). This difference in the sequence order is due to the manner of the projection of the potential in the slices. The projection of the potential onto the front surface of the slice leads to (13*b*) while that onto the rear surface leads to the Cowley–Moodie equation. However, the difference in the final result of the multislice calculation is negligible when a large number of slices are taken into account.

The following conclusion may be drawn from the above derivation of the multislice formula. The potential distribution should vary slowly over the distance $(\Delta z/k)^{1/2}$ or $\Delta z\,.\,\alpha$, where Δz denotes the slice thickness (*i.e.* $\Delta z=z-z_0$). These conditions are almost identical to

$$\Delta z\lesssim kd^2, \quad (15)$$

since $\alpha\simeq 1/kd$, where d is the distance over which the potential does not not change by an appreciable fraction. In the high-voltage limit where k becomes infinite, the whole potential can be projected, so that

$$\varphi_z(\mathbf{b})=\exp\left\{-\frac{i}{\hbar v}\int_{z'=-\infty}^{z'=z}V(\mathbf{b},z')\mathrm{d}z'\right\}, \quad (16)$$

which is identical to the Glauber (1953) approximation for high-energy scattering. Equation (16) will be denoted as a thin-phase-grating approximation, because the specimen is seen as a *thin* object by the high-energy electrons. It should be noted that even at the highest accelerating voltage the condition of the Born approximation:

$$V(\mathbf{r})\Delta z/\hbar v\ll 1$$

may not be satisfied in the case of the thick specimen, because the value of $\hbar v$ never exceeds the limiting value $\hbar c$ (equal to 1973 eV Å), where c is the velocity of light.

2.2 *Scattering amplitudes*

For small-angle scattering, such as in the case of high-energy electrons, the scattering amplitudes are given by the Fourier transform of the wave function $\varphi(\mathbf{b},z)$ at the bottom surface of specimen as follows:

$$\begin{aligned}F(\mathbf{k},\mathbf{k}')&=\frac{1}{\lambda i}\int[\exp i(\mathbf{k}-\mathbf{k}')\mathbf{r}]\{\varphi(\mathbf{b},z)-1\}\mathrm{d}\mathbf{b}\\&=-\frac{2m}{4\pi\hbar^2}\int\int V(\mathbf{b}',z')\varphi(\mathbf{b}',z')\exp i(\mathbf{k}-\mathbf{k}')z\mathbf{e}\\&\times\frac{1}{z-z'}\frac{1}{\lambda i}\left[\int\exp i\left\{(\mathbf{k}-\mathbf{k}')\mathbf{b}+\frac{k|\mathbf{b}-\mathbf{b}'|^2}{2(z-z')}\right\}\mathrm{d}\mathbf{b}\right]\mathrm{d}\mathbf{b}'\mathrm{d}z', \quad (17a)\end{aligned}$$

where $\mathbf{k}$ and $\mathbf{k}'$ are the wavevectors of the incident and the scattered electrons respectively, and $\mathbf{e}$ denotes the unit vector along the z direction. When the integral over the plane of $\mathbf{b}$ is carried out, then

$$\begin{aligned}&\frac{1}{z-z'}\frac{1}{\lambda i}[\ldots]\\&\quad=\exp[i(\mathbf{k}-\mathbf{k}')\mathbf{b}']\exp\{-i|\mathbf{k}-\mathbf{k}'|^2/[2k/(z-z')]\}.\end{aligned}$$

When the small-angle approximation holds and $kZ\alpha^4/4\ll 1$, then

$$\begin{aligned}&\exp\{-i(\mathbf{k}-\mathbf{k}')(z-z')\mathbf{e}\}\\&\qquad\simeq\exp\{-i|\mathbf{k}-\mathbf{k}'|^2/[2k/(z-z')]\},\end{aligned}$$

where Z is the specimen thickness. Thus (17*a*) reduces to

$$F(\mathbf{k},\mathbf{k}')=-\frac{2m}{4\pi\hbar^2}\int V(\mathbf{r})\varphi(\mathbf{r})[\exp i(\mathbf{k}-\mathbf{k}')\mathbf{r}]\mathrm{d}\mathbf{r}\,, \quad (17b)$$

which corresponds to the definition of the scattering amplitudes.

III. Computation procedure

The convolution integral (equation 13*b*) is to be computed in the multislice method. Goodman & Moodie (1974) summarized the practical procedure of the direct calculation of the convolution integral. In this present work a set of new computer programs is devised. The convolution is now calculated through the two-dimensional fast Fourier transform (FFT) which is carried out by the successive application of the one-dimensional FFT algorithm (*e.g.* Brigham, 1974). The computation time for the convolution is mainly determined by the number of multiplications. If N_1 and N_2 are the number of beams (or sampling points) along the two axes respectively, the computation time of one FFT is proportional to

$$N_2(N_1\log_2 N_1)+N_1(N_2\log_2 N_2)=N\log_2 N$$

where $N=N_1N_2$. Here N_1 and N_2 must be chosen to be the powers of 2 in the base-2-FFT algorithm. Then

the computing time for one multislice cycle in this procedure is proportional to

$$2(N \log_2 N)+2N=2N \log_2 2N$$

as seen from Fig. 2, while one cycle of multislice calculation based on the direct convolution requires a computation time proportional to $N^2+N\simeq N^2$. The use of the present programs makes it possible to include about 8000 beams within a moderate computing time which may correspond to the time of the direct convolution of about 500 beams. The wavefunctions, as well as the scattering amplitudes, are calculated in the present computation scheme to give some physical insight in terms of real-space quantities.

The newly developed programs are suitable for the crystal arrangement where coherent illumination is assumed. Each slice is occupied by the same number of unit cells along the incident electron direction (identical to the c axis of the crystal), so that the propagation function and the phase-grating function are identical for each slice. These functions are calculated in advance of the multislice cycle. The propagation function P in reciprocal space is used in the present programs, and calculated through the following equation (Goodman & Moodie, 1974):

$$P(h,k)=\exp\left\{-2\pi i\Delta z\frac{\lambda}{2}\left[\left(\frac{h}{a}\right)^2+\left(\frac{k}{b}\right)^2\right]\right\}, \quad (18)$$

where h and k are integers representing the reciprocal lattice points of the rectangular cell of dimensions a and b. The phase-grating function q is directly calculated with (14b) from the projected potential. The projection of the potential along the c axis of the crystal is synthesized by the FFT program through the following Fourier projection theorem:

$$V_p(x,y)=\frac{1}{a\times b}\sum_h\sum_k F(h,k,0)\exp\left[2\pi i(hx+ky)\right], \quad (19)$$

where $F(h,k,0)$ is calculated from the atomic scattering factors (*International Tables for X-ray Crystallography*, 1974) for the model specimen.†

The convolution (equation 13b) is carried out by the use of the Fourier theorem of convolution:

$$\mathcal{F}\{[\varphi_n . q] * p\}=\mathcal{F}\{\varphi_n . q\}.\mathcal{F}\{p\},$$

so that

$$\varphi_{n+1}=\mathcal{F}\{\varphi_n . q\} . P . \quad (20)$$

A simple FFT algorithm adopted in the present program requires that the number of sampling points of the input function must be equal to that of the transformed output function. The corresponding unit-cell edge is thus divided into $2H$ points for the $2H$ beams from $-H$ to $H-1$ along one axis. The wavefunction and the scattering amplitudes calculated by the present scheme are self-normalized according to Parseval's theorem for a pure phase object (*i.e.* a specimen with no absorption). The square sum of these amplitudes is independent of the slice number n:

$$\sum_{X=0}^{N_1-1}\sum_{Y=0}^{N_2-1}\left|\varphi_n\left(\frac{X}{N_1},\frac{Y}{N_2}\right)\right|^2=\sum_X\sum_Y\left|\varphi_{n+1}\left(\frac{X}{N_1},\frac{Y}{N_2}\right)\right|^2,$$

$$\sum_{H=-N_1/2}^{N_1/2-1}\sum_{K=-N_2/2}^{N_2/2-1}|\Phi_n(H,K)|^2=\sum_H\sum_K|\Phi_{n+1}(H,K)|^2.$$

When the sampling intervals are too coarse to detect the specimen structure, an aliasing effect (the overlapping of the waveform; Brigham, 1974) occurs in a discrete Fourier transform such as the FFT. Thus a sufficient number of sampling points (or beams) should be taken to avoid the aliasing effect.

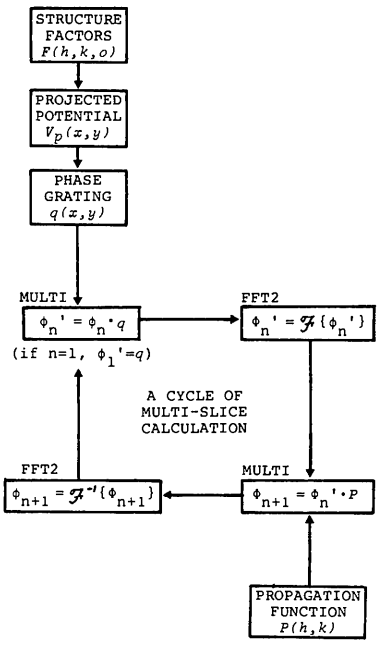

Fig. 2. A flow chart of the procedure for the multislice calculation. Here the capital letters Φ and P denote the Fourier transforms of the corresponding functions φ and p respectively. The phase grating q and propagation function P are computed in advance of the multislice iteration.

IV. Applications

Multislice calculations based on the present technique are applied to the electron scattering of chlorinated Cu-phthalocyanine (Uyeda & Ishizuka, 1974). Its crystal data are:

$$a=19{\cdot}62,\ b=26{\cdot}04,\ c=3{\cdot}76\ \text{Å},\ \beta=116{\cdot}5°.$$

The accelerating voltages for the incident electrons are assumed to be 100 and 500 kV. The wavefunctions and

† In the present scheme of the multislice calculation the phase grating q in real space is used, while Goodman & Moodie (1974) use its Fourier transform Q in reciprocal space. The present method of calculating q by means of the FFT has the same advantage as Lynch's (1974) method of evaluating Q directly from the $F(h,k,0)$ as discussed by him.

the scattering amplitudes are calculated as functions of either the number of beams or the slice thickness. The kinematical results as well as the results of the thin-phase-grating approximation are given in §4.2. The probability distributions of electrons are calculated to estimate the maximum specimen thickness for which the simple relations with the specimen structure can be maintained.

4.1 *Phase-grating calculation*

Two sets of the phase-grating functions were calculated in advance of the multislice iteration in order that the effect of the number of beams and the slice thickness in the multi-slice algorithm could be estimated. A set of the phase-gratings q was evaluated from the projected potentials calculated for 100 kV electrons with various numbers of beams as summarized in Table 1 with the slice thickness of one unit cell (3·76 Å) assumed. The non-linear effect of V_p on q is relatively small in this case, since $(V_p)_{max}/\hbar v \simeq 360/1082$ (0·33) at the centre of the copper atom ($\hbar v = 1082$ eV Å for 100 kV electrons). Here, the low-resolution projected potential calculated with a small number of beams such as 16×32 or 32×64 gives the low-resolution phase grating, but its Fourier transform Q is almost equal to the most accurate one calculated from 64×128 beams. Table 2 shows the power spectrum of the phase grating of 64×128 beams *vs* $2(\sin\theta/\lambda)$. It can be seen that the beams up to $2(\sin\theta/\lambda) \simeq 1{\cdot}8$ Å^{-1} must be included in order to give a sufficiently accurate phase grating for the present model specimen with slice thickness of one unit cell, although the phase grating calculated from the small number of beams gives at least an approximate result for the phase grating *per se*.

Table 2. *Power spectrum of a one-unit-slice phase grating for* 100 kV *electrons*

$2(\sin\theta/\lambda)$	Number of beams	Fraction
0·0–0·2	57	0·998590
0·2–0·4	174	0·000550
0·4–0·6	288	0·000476
0·6–0·8	394	0·000206
0·8–1·0	522	0·000137
1·0–1·2	638	0·000025
1·2–1·4	744	0·000010
1·4–1·6	862	0·000004
1·6–1·8	972	0·000002
1·8–2·0	907	0·000000

Another set of phase-grating functions was obtained for 500 kV electrons with various slice thicknesses of 2, 4, 10 and 20 unit cells. The number of beams is kept constant at about 8000 (64×128 beams with about 4000 allowed beams) in these calculations. More beams are needed to represent q accurately with increasing slice thickness, because the non-linear effect of V_p becomes appreciable, as pointed out by Lynch & O'Keefe (1972). The power spectra of these phase gratings shown in Table 3 have guaranteed that the number of beams was sufficient for slice thicknesses up to 20 cells.

Table 1. *Some conditions for various numbers of beams with chlorinated* Cu-*phthalocyanine*

Case	Number of beams (allowed*)	Maximum index h ; k	Maximum $2\sin\theta/\lambda$ (Å^{-1}) a^* ; b^*	Sampling interval (Å) a/N_1 ; b/N_2
(1) 16×32	512 (256)	8 ; 16	0·46 ; 0·61	1·10 ; 0·81
(2) 32×64	2048 (1024)	16 ; 32	0·91 ; 1·23	0·55 ; 0·41
(3) 64×64	4096 (2048)	32 ; 32	1·82 ; 1·23	0·27 ; 0·41
(4) 64×128	8192 (4096)	32 ; 64	1·82 ; 2·46	0·27 ; 0·20

* Possible reflexions allowed by the specimen symmetry *cmm*.

Table 3. *Power spectra of phase gratings with various slice thicknesses for* 500 kV *electrons* (64×128 *beams*)

$2(\sin\theta/\lambda)$	Number of beams	Fraction of power spectra ($\times 10^6$) 2 cells	4 cells	10 cells	20 cells
0·0–0·2	57	997764	991146 (991104)*	948087 (946182)*	832456 (808118)*
0·2–0·4	174	871	3432 (3465)	19407 (20908)	54826 (73850)
0·4–0·6	288	753	2984 (3006)	17372 (18381)	54590 (67766)
0·6–0·8	394	328	1296 (1303)	7637 (7956)	24908 (28983)
0·8–1·0	522	219	871 (869)	5411 (5159)	20456 (16834)
1·0–1·2	638	39	156 (153)	1092 (894)	5425 (2891)
1·2–1·4	744	17	70 (66)	550 (355)	3316 (1052)
1·4–1·6	862	7	31 (28)	280 (123)	2089 (366)
1·6–1·8	972	2	8 (6)	103 (30)	1056 (104)
1·8–2·0	907	0	3 (1)	38 (8)	477 (27)
2·0–2·2	812	0	0 (0)	16 (3)	228 (8)
2·2–2·4	766	0	0 (0)	5 (0)	105 (2)
2·4–2·6	607	0	0 (0)	3 (0)	46 (0)
2·6–2·8	304	0	0 (0)	0 (0)	17(0)
2·8–3·0	145	0	0 (0)	0 (0)	6 (0)

* Power spectrum of multislice result at the same thickness.

4.2 *Multislice iteration*

4.2(*a*) *Effect of number of beams*

The first set of phase gratings obtained in §4.1 was used in multislice iteration. The slice thickness was kept constant at one unit cell, and the incident electron beam was assumed normal to the reciprocal net plane. Fig. 3 shows the typical results for the scattering amplitudes for various numbers of beams. The calculated value is supposed to approach the limiting value of an analytical integration as the number of beams is increased. As seen in Fig. 3, the results for 64×64 beams and 64×128 beams show only slight differences up to a crystal thickness of 100 cells. The sum of differences of Φ_A and Φ_B is defined as a measure of convergence to the limiting value:

$$R(HK) = \frac{\sum_{h=0}^{H} \sum_{k=0}^{K} \left| |\Phi_A(hk)| - |\Phi_B(hk)| \right|}{\sum_{h=0}^{H} \sum_{k=0}^{K} \{|\Phi_A(hk)| + |\Phi_B(hk)|\}} .$$

The value of $R(16,8)$ is less than 0·012 for each slice up to 100 cells in the case of 64×64 and 64×128 beams. These results are thus close to the limiting value of the scattering amplitudes below this crystal thickness. The result for 32×64 beams, however, starts to deviate from the estimated limiting value at about the specimen thickness of 50 cells (190 Å), although the calculation includes about 1000 beams allowed by the specimen symmetry of *cmm*. The results for 16×32 beams deviate from the limiting value at an early stage of multislice iteration. This deviation is especially noticeable in the results for a weak reflexion such as 150 or for off-centre reflexions such as 800, 0,16,0 and 8,16,0 as seen from Fig. 3. The failure in multislice iteration is appreciable in the case of 32×64 beams and is drastic in the case of 16×32 beams.

4.2(*b*) *Effect of slice thickness*

In order to estimate the upper limit of slice thickness in the multislice calculation, computations were carried out for 500 kV electrons with the second set of phase-grating functions obtained in §4.1. In these calculations the same slice thickness and number of beams were used as in estimating each phase grating. The scattering amplitudes for various slice thicknesses are shown in Fig. 4. The results for the slices of two and four cells are almost the same and the value of $R(32,64)$ is less than 0·007 up to the crystal thickness of 200 cells, so that these results are close to the limiting value, which will be obtained by the calculation with an infinitesimal slice thickness. The slice thickness Δz of four cells is equal to 15·0 Å. The condition of the stationary-phase approximation (equation 15) will be satisfied with the d value of 0·2 Å since $k = 442$ Å^{-1} for 500 kV electrons. In the case of 100 kV electrons ($k = 170$ Å^{-1}), the approximate limiting value was obtained with the slice thickness of two cells (7·5 Å).

An approximate result can be obtained through the calculation with thicker slices, as shown in Fig. 4, when the pseudo-upper-layer interaction is small. The parameter for the pseudo-upper-layer interaction is defined (Goodman & Moodie, 1974):

$$\alpha(hk) = -\zeta(hk) \,.\, \Delta z; \quad -\zeta(hk) = \frac{\lambda}{2}\left\{\left(\frac{h}{a}\right)^2 + \left(\frac{k}{b}\right)^2\right\}.$$

The values of $-\zeta$ for the reflexions in Fig. 4(*a*)–(*f*), are 0·0, $0{\cdot}133 \times 10^{-3}$, $0{\cdot}372 \times 10^{-3}$, $0{\cdot}279 \times 10^{-3}$, $0{\cdot}415 \times 10^{-2}$ and $0{\cdot}166 \times 10^{-1}$ Å^{-1} respectively. $\alpha(hk)$ is proportional to the slice thickness Δz. The reflexion where $\alpha(hk) < 0{\cdot}5$ reflects the general pattern of the limiting scattering amplitudes as concluded from the results for slice thicknesses of 10 and 20 cells. The effect of the pseudo-upper-layer interaction is seen in the reflexion in Fig. 4(*f*) in the calculation of 20 cells slice thickness where $\alpha(16,32)$ is equal to 1·25. These results confirm that the rapid calculation with thicker slices gives at least approximately correct scattering amplitudes. The result based on the thin-phase-grating approximation (equation 16) did not agree with the limiting value of the multislice calculation when the crystal thickness exceeded 20 cells (75 Å) for 500 kV electrons. This critical thickness may be reduced to one half for 100 kV electrons, because the factor $h\nu$ in (16) is reduced from 1703 to 1082 eV Å when the accelerating voltage changes from 500 to 100 kV.

4.3 *Wavefunctions*

The wavefunctions are obtained as a function of the specimen thickness in the course of the calculation with the present program, in addition to the scattering amplitudes. Fig. 5 shows some results of the intensity distribution of the wave function (*i.e.* the probability distribution of the electrons) at the indicated crystal thickness. They were calculated for 500 kV electrons with the slice thickness of two cells in the 64×128 case [see §4.2(*b*)]. In these figures, lighter coloured regions show a higher electron density. Since the model specimen is assumed to be a pure phase object, the electron density difference for crystals thinner than 10 unit cells is relatively small. When the crystal thickness is over 40 cells, it is seen that electrons converge into each atom position and the dark areas of the electron density appear in the surrounding regions. This phenomenon can be compared to the action of a convex lens positioned at each atom location. Fig. 6 shows the probability density at the positions of copper, chlorine and nitrogen atoms as a function of specimen thickness. The oscillations of intensity with specimen thickness can be seen in the scattering amplitudes shown in Figs. 3 and 4, and also in the electron densities of the scattered waves in Fig. 6. The wavefunction is quantitatively analysed in terms of the specimen structure when the probability distribution of the scattered electrons is proportional to the specimen thickness. The thickness of 40 cells (150 Å) seems to be the critical value for 500 kV electrons, below which the proportionality between the probability density and the

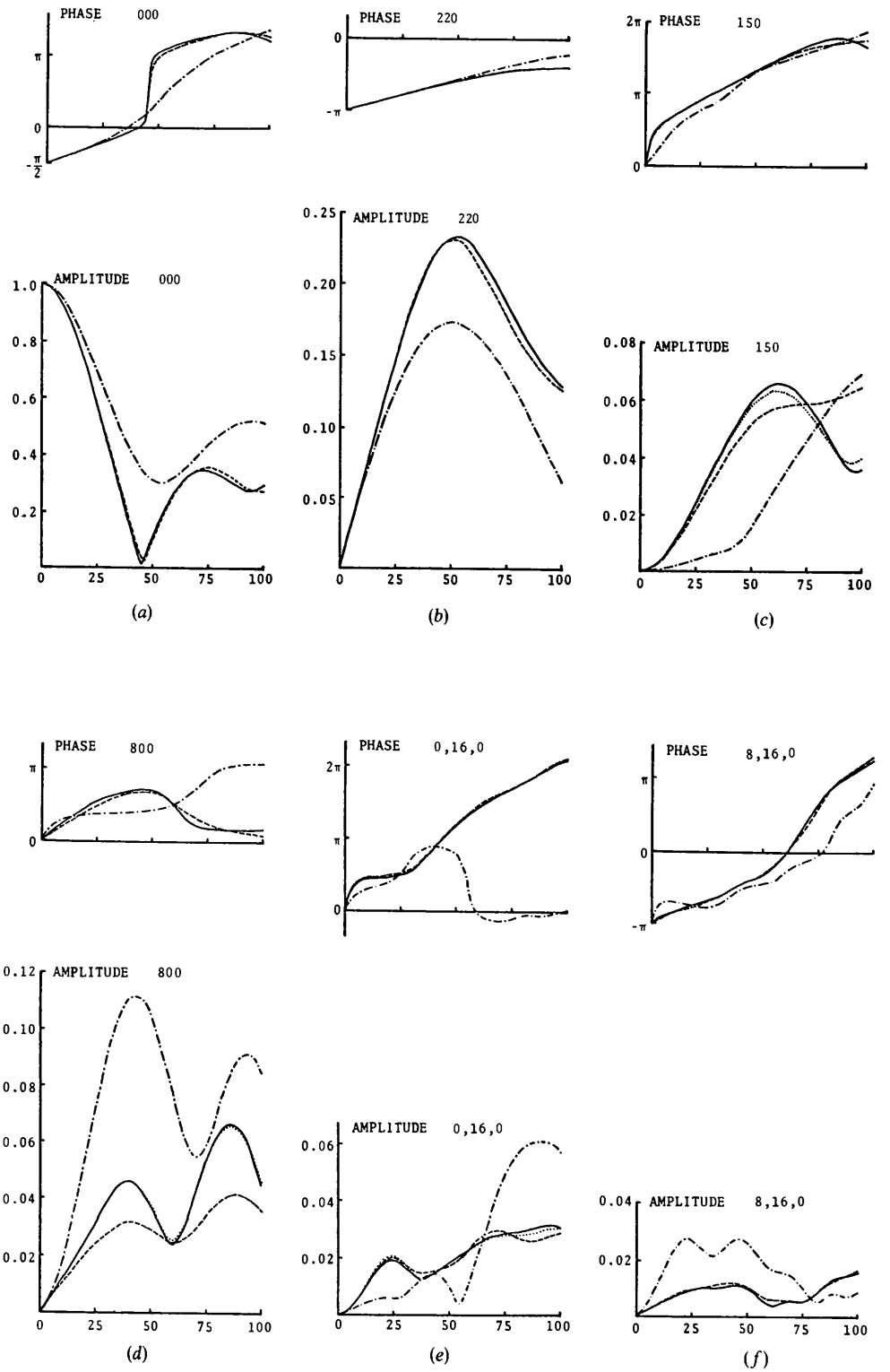

Fig. 3. Scattering amplitudes (and phases) calculated for 100 kV electrons as a function of the specimen thickness (number of cells) with various numbers of beams: 64×128 beams (solid line), 64×64 beams (dotted line), 32×64 beams (dashed line) and 16×32 beams (chain line). (*a*) shows the change of the main beam, (*b*) and (*c*) show a strong and a weak reflexion respectively. (*d*) to (*f*) give the examples of off-centre reflexions. The results for the amplitudes of the reflexions (*a*), (*b*) and (*f*) and that for the phase of all (*a*) to (*f*) for 64×64 beams are almost equal to those for 64×128 beams. The phase of reflexion (*b*) for 32×64 beams is almost equal to the results for 64×128 and 64×64 beams.

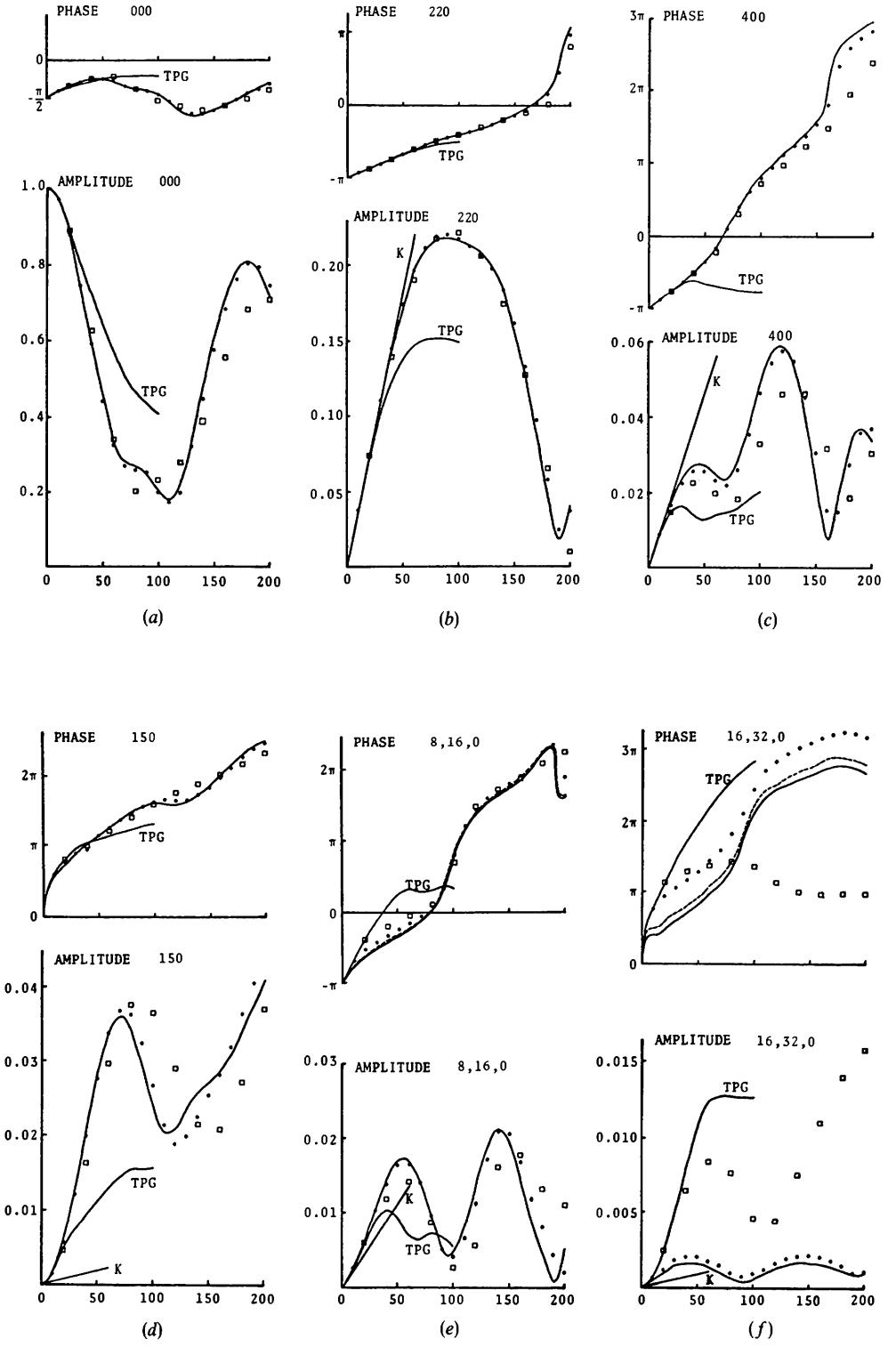

Fig. 4. Scattering amplitudes (and phases) calculated for 500 kV electrons as a function of the specimen thickness. The results of the multislice calculation with the slice thickness of two cells (solid line), four cells (dashed line), 10 cells (dots) and 20 cells (squares) are shown. (*a*) shows the change of the main beam, (*b*) that of a strong beam, and (*c*) and (*d*) that of a weak beam. (*e*) and (*f*) show the change of the beam scattered in the direction of the off-centre part. The amplitudes for the slice thickness of two and four cells are almost identical for all (*a*) to (*f*). The phase for the slice thickness of four cells is almost equal to that for two cells except for reflexions (*e*) and (*f*). The results based on the kinematical theory (solid straight line denoted by K) and the thin-phase-grating approximation (solid line denoted by TPG) are also shown for each reflexion.

specimen thickness is maintained. The critical thickness for 100 kV electrons was found to be about 30 cells (100 Å). The critical thickness will be lower for the specimen containing heavy atoms, since the oscillating behaviour of the electron density at the position of the heavier atom is seen at a smaller specimen thickness.

V. Discussion

The following conditions are required for the derivation of the multislice formula:

(*a*) $\alpha^2 \ll 1$, for the maximum scattering angle,

(*b*) $\Delta z \lesssim kd^2$, for the maximum slice thickness, and for the scattering amplitude calculation:

(*c*) $kZ\alpha^4/4 \ll 1$, for the specimen thickness and the scattering angle of each reflexion.

The condition (*a*) is usually satisfied except in LEED experiments. The condition (*b*) restricts the maximum slice thickness, which is proportional to the wavenumber of the incident electrons and influenced by the rate of the potential change through the parameter *d*. The correct value of the scattering amplitudes will be obtained under the condition (*c*) which gives the relation between the specimen thickness and the scattering angle of each reflexion. Although the slice thickness is restricted by the condition (*b*), there is no restriction on the number of beams in the multislice calculation.

The number of beams required to obtain an accurate result in multislice iteration will be determined by the specimen structure, which defines the scattering property of each slice. Another important factor determining the number of beams is the final specimen thickness, since each convolution in a multislice iteration usually requires a greater number of beams (or sampling points) than those of the two convoluting functions. When the number of beams is not sufficient, the aliasing effect will be appreciable in each convolution based on FFT. Thus the number of beams required will be larger as the specimen thickness increases. For the same reason, the number of beams in multislice iteration must be no less than the number of the sampling points in the phase grating. It should be noted that the number of beams required in the final multislice iteration does not depend on the slice thickness, if the number of sampling points in the phase grating is sufficient. The number of sampling points in the phase grating, however, is affected by the slice thickness and the specimen structure. When the slice thickness is small enough for the non-linear effect of the projected potential to be neglected, the required number of sampling points in the phase grating is approximately equal to that of the projected potential. The number of sampling points should be increased for the thicker-slice phase grating, since the non-linear effect becomes appreciable.

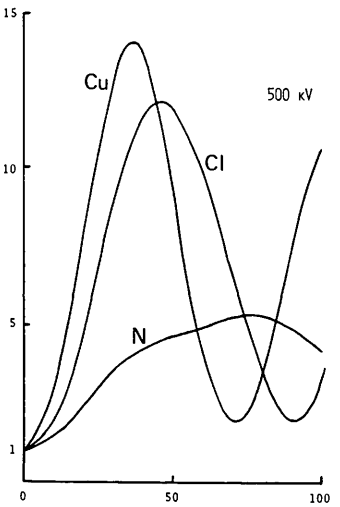

Fig. 6. Intensity distribution of the wavefunction calculated for 500 kV electrons as a function of the specimen thickness. The values at the positions of copper, chlorine and nitrogen atoms are shown. The oscillating behaviour of the intensity of the heavier atom is seen at a smaller specimen thickness.

The following conclusions will be drawn from the above discussions and the results of calculations based on the model specimen, chlorinated Cu-phthalocyanine.

(1) The number of beams for the multislice calculation based on the FFT algorithm should be no less than the number of sampling points which represent the correct projected potential. In order to represent the projected potential with sufficient accuracy, the unit-cell edges should be divided into 0·25 to 0·30 Å intervals, which correspond to a scattering vector $2(\sin\theta/\lambda)$ of $1{\cdot}6 \sim 2{\cdot}0$ Å^{-1}. This value is not much affected by the wavelength of the incident electrons and the specimen structure. The multislice calculation with the low-resolution phase-grating function fails because of the aliasing effect of the convolution during the multislice iteration.

(2) The maximum slice thickness is about kd^2, where d is chosen to be about 0·2 Å. This value d does not depend on the specimen except when it contains very heavy atoms. The failure in the multislice calculation with thicker slices is due to the use of an exceedingly thick phase grating, which is already different from the multislice result, as seen from Table 3. The stationary-phase approximation (equation 15) holds to about a slice ten times thicker than that which the Born approximation requires. The specimen thickness in the present model should be far less than 18 and 11 Å for 500 and 100 kV electrons respectively to satisfy the condition of the Born approximation.

(3) The effect of multiple scattering on the wavefunction becomes serious when the specimen thickness exceeds its critical value. The linear relationship between the probability distribution of electrons and the specimen structure holds in the range below this critical thickness. These values are 150 and 100 Å for

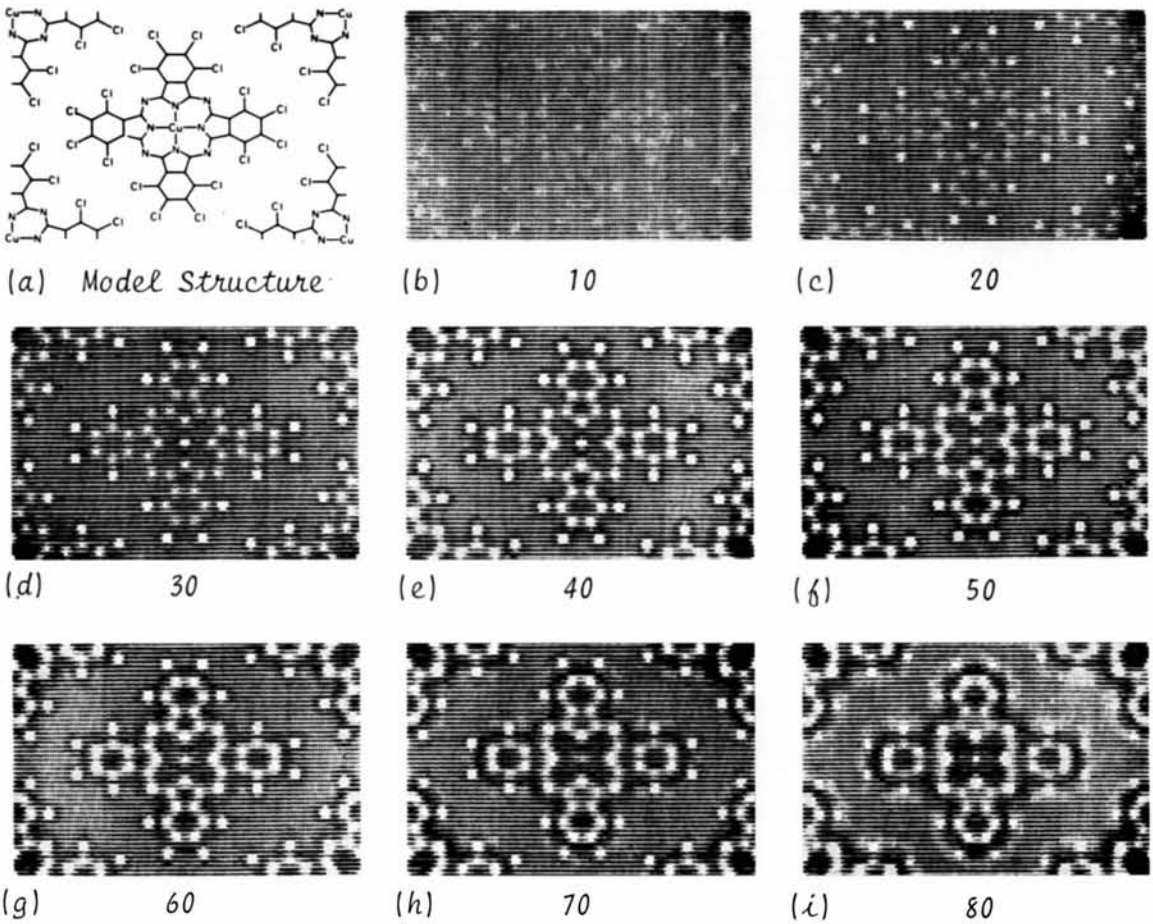

FIG. 5. The model structure (*a*) and the intensity distributions of the wave function (*b*) to (*i*), calculated for 500 kV electrons with the indicated specimen thickness (number of cells). The model specimen is assumed to be a pure phase object. Lighter regions show a higher electron density.

[*To face p.* 748

500 and 100 kV electrons respectively in the case of the present model specimen.

We would like to acknowledge Dr J. V. Sanders, CSIRO Division of Tribophysics, for an informative discussion about the results of the Australian school. Thanks are due to Dr M. A. O'Keefe for his stimulating criticism and discussion. Thanks are also due to Dr K. Kajiwara for critical reading of the manuscript. We are grateful to Data Processing Center, Kyoto University and Hokkaido Computing Center for the provision of excellent computing facilities.

This work was supported by the Grand-in Aid for Scientific Research, Ministry of Education, Japan, which is grately acknowledged. One of us (KI) would like to thank the Matsunaga Science Foundation for a financial support.

APPENDIX

1. Evaluation of equation (11)

From the definition of the propagation function,

$$p(\mathbf{b}'-\mathbf{b}_0,z'-z_0)p(\mathbf{b}-\mathbf{b}',z-z')=\frac{1}{(\lambda i)^2}\frac{1}{(z'-z_0)(z-z')}$$
$$\times\exp\left\{ik\frac{|\mathbf{b}-\mathbf{b}_0|^2}{2(z-z_0)}\right.$$
$$\left.+ik\frac{z-z_0}{2(z'-z_0)(z-z')}\left|\mathbf{b}'-\frac{(z'-z_0)\mathbf{b}+(z-z')\mathbf{b}_0}{z-z_0}\right|^2\right\}.$$

The integration over $\mathbf{b}'$ is carried out by the method of stationary phase (Eckart, 1948). When the potential distribution does not change appreciably over a distance of the order of

$$\left\{\frac{2(z'-z_0)(z-z')}{k(z-z_0)}\right\}^{1/2}\text{ bounded by }\left\{\frac{z-z_0}{2k}\right\}^{1/2},\quad(A1)$$

then

$$\int V(\mathbf{b}',z')p(\mathbf{b}'-\mathbf{b}_0,z'-z_0)p(\mathbf{b}-\mathbf{b}',z-z')\mathrm{d}\mathbf{b}'$$
$$\simeq V\left(\frac{(z'-z_0)\mathbf{b}+(z-z')\mathbf{b}_0}{z-z_0}\right)$$
$$\times\int p(\mathbf{b}'-\mathbf{b}_0,z'-z_0)p(\mathbf{b}-\mathbf{b}',z-z')\mathrm{d}\mathbf{b}'$$
$$=V\left(\frac{(z'-z_0)\mathbf{b}+(z-z')\mathbf{b}_0}{z-z_0}\right)p(\mathbf{b}-\mathbf{b}_0,z-z_0).\quad(A2)$$

2. Verification of equation (12*b*)

This equation is proved by mathematical induction as follows. If f_n satisfies (12*b*), then f_{n+1} will be obtained from (10*b*):

$$f_{n+1}(\mathbf{b},z)$$
$$=\int\int_{z'=z_0}^{z'=z}V(\mathbf{b}',z')\left\{\int\frac{1}{n!}\left[\int_{z''=z_0}^{z''=z'}V(\mathbf{b}_0,z'')\mathrm{d}z''\right]^n\right.$$
$$\left.\times\varphi(\mathbf{b}_0,z)p(\mathbf{b}'-\mathbf{b}_0,z'-z_0)\mathrm{d}\mathbf{b}_0\right\}p(\mathbf{b}-\mathbf{b}',z-z')\mathrm{d}z'\mathrm{d}\mathbf{b}'.\quad(A3)$$

By the same method as used to give (*A*2), f_{n+1} becomes

$$f_{n+1}(\mathbf{b},z)$$
$$=\int\left\{\int\int_{z'=z_0}^{z'=z}V(\mathbf{b}_0,z')\frac{1}{n!}\left[\int_{z''=z_0}^{z''=z'}V(\mathbf{b}_0,z'')\mathrm{d}z''\right]^n\mathrm{d}z'\right\}$$
$$\times\varphi(\mathbf{b}_0,z_0)p(\mathbf{b}-\mathbf{b}_0,z-z_0)\mathrm{d}\mathbf{b}_0.\quad(A4)$$

The integration over z' in the curly brackets is carried out by parts:

$$\frac{1}{n!}\int_{z'=z_0}^{z'=z}V(\mathbf{b}_0,z')\left[\int_{z''=z_0}^{z''=z'}V(\mathbf{b}_0,z'')\mathrm{d}z''\right]^n\mathrm{d}z''$$
$$=\frac{1}{(n+1)!}\left[\int_{z'=z_0}^{z'=z}V(\mathbf{b}_0,z')\mathrm{d}z'\right]^{n+1}.\quad(A5)$$

f_{n+1} is finally found in the desired form:

$$f_{n+1}(\mathbf{b},z)=\int\frac{1}{(n+1)!}\left[\int_{z'=z_0}^{z'=z}V(\mathbf{b}_0,z')\mathrm{d}z'\right]^{n+1}$$
$$\times\varphi(\mathbf{b}_0,z_0)p(\mathbf{b}-\mathbf{b}_0,z-z_0)\mathrm{d}\mathbf{b}_0.\quad(A6)$$

With equation (12*a*) and this equation the mathematical induction is completed.

References

ALLPRESS, J. G., HEWAT, E. A., MOODIE, A. F. & SANDERS, J. V. (1972). *Acta Cryst.* A**28**, 528–536.
ANSTIS, G. R., LYNCH, D. F., MOODIE, A. F. & O'KEEFE, M. A. (1973). *Acta Cryst.* A**29**, 138–147.
BRIGHAM, E. O. (1974). *The Fast Fourier Transform.* New York: Prentice-Hall.
COWLEY, J. M. & MOODIE, A. F. (1957). *Acta Cryst.* **10**, 609–619.
ECKART, C. (1948). *Rev. Mod. Phys.* **20**, 399–417.
FUJIWARA, K. (1959). *J. Phys. Soc. Japan*, **14**, 1513–1524.
GLAUBER, R. J. (1953). *Phys. Rev.* **91**, 459.
GOODMAN, P. & MOODIE, A. F. (1974). *Acta Cryst.* A**30**, 280–290.
International Tables for X-ray Crystallography (1974). Vol. IV, pp. 155–163. Birmingham: Kynoch Press.
LYNCH, D. F. (1974). *Acta Cryst.* A**30**, 101–102.
LYNCH, D. F., MOODIE, A. F. & O'KEEFE, M. A. (1975). *Acta Cryst.* A**31**, 300–307.
LYNCH, D. F. & O'KEEFE, M. A. (1972). *Acta Cryst.* A**28**, 536–548.
MARGENAU, H. & MURPHY, G. M. (1943). *The Mathematics of Physics and Chemistry*, Chap. XIV. New York: Van Nostrand Company.
O'KEEFE, M. A. (1973). *Acta Cryst.* A**29**, 389–401.
O'KEEFE, M. A. & SANDERS, J. V. (1975). *Acta Cryst.* A**31**, 307–310.
SCHIFF, L. I. (1956). *Phys. Rev.* **103**, 443–453.
UYEDA, N. & ISHIZUKA, K. (1974). *J. Electron Microsc.* **23**, 79–88.